A Complete Statistical Investigation of RTN in HfO_2-Based RRAM in High Resistive State

Francesco Maria Puglisi, *Student Member, IEEE,* Luca Larcher, *Member, IEEE,* Andrea Padovani, *Member, IEEE,* Paolo Pavan, *Senior Member, IEEE*

***Abstract*—In this paper we investigate the Random Telegraph Noise (RTN) in hafnium-oxide Resistive Random Access Memories (RRAMs) in High Resistive State (HRS). The current fluctuations are analyzed by decomposing the multi-level RTN signal into two-level RTN traces using a Factorial Hidden Markov Model (FHMM) approach, which allows extracting the properties of the traps originating the RTN. The current fluctuations, statistically analyzed on devices with different stack reset at different voltages, are attributed to the activation and de-activation of defects in the oxidized tip of the conductive filament, assisting the TAT transport in HRS. The physical mechanisms responsible for the defect activation are discussed. We find that RTN current fluctuations can be due to either i) the coulomb interaction between oxygen vacancies (normally assisting the charge transport) and the electron charge trapped at interstitial oxygen defects, or ii) the metastable defect configuration of oxygen vacancies assisting the electron transport in HRS. A consistent microscopic description of the phenomenon is proposed, linking the material properties to the device performance.**

***Index Terms*—RTN, Variability, Cycling, RRAM, Noise.**

I. Introduction

RESISTIVE random access memories (RRAMs) based on transition metal oxides (TMO) are presently among the most appealing emerging non-volatile memories (NVMs), demonstrating reliable and fast switching, low-power operation, and high-density [1-4]. RRAMs switching relies on the formation and partial oxidation of a conductive filament (CF) during set and reset operations, respectively [5]. The CF formation drives the device in low-resistance state (LRS) while its partial oxidation creates a dielectric barrier, which determines the high-resistance state (HRS) [6]. LRS exhibits quasi-ohmic behavior [5], while charge transport in HRS is dominated by a multi-phonon trap-assisted tunneling (TAT) process [7] via the O vacancy defects in the barrier. The intrinsic randomness of the physical mechanisms of the reset and set operations results in cycling variability of both HRS and LRS resistances, which should be included in compact models for variability-aware design of RRAM-based circuits [8-10]. Another intrinsic variability source affecting the RRAM behavior during reading is the Random Telegraph Noise (RTN) [11-19]. The current value measured during reading operation shows sudden sharp fluctuations, critical in HRS and less hazardous in LRS. The RTN disturb represents today one of the most significant limitations for the full exploitation of RRAM technology. It may indeed reduce the readout margin of the device and cause read failures. Papers by a number of research groups have investigated RTN in HfO_2-based RRAM. Unfortunately, only few addressed the complex multi-level RTN characteristics [11], and in most cases the measurement interpretation did not account for the TAT [14-16], which dominates the charge transport in HRS. A truthful description of RTN has to analyze multi-level RTN in the framework of the TAT model. In this work, we explore RTN features in HRS through an extensive noise characterization of RRAM devices with different stack compositions. Statistical properties of traps contributing to the multi-level RTN are retrieved by analyzing RTN through the FHMM method [17, 18]. Results suggest that the activation and de-activation of O vacancies defects supporting TAT, due to either the Coulomb blockade effect or the metastable defect switching, are responsible for RTN.

This paper is organized as follows. The description of the devices and measurements is given in Section II. The RTN fluctuations analysis is introduced in Section III. The results of noise analysis in terms of dependence on the reset voltage and correlation with the cycling variability are discussed in Section IV. In Section V, the physical mechanisms responsible for RTN are discussed. Statistical considerations linking the structural properties of the device to the RTN features are drawn in Section VI. Conclusions follow.

II. Devices and Experiments

Measurements are performed on TiN/Ti/HfO_x/TiN RRAM devices with different areas (from 50x50 to 200x200 nm^2), and Ti (5 and 6 nm) and HfO_x (4.2 and 5 nm) thicknesses. The Ti layer stacked on top of the hafnium oxide acts as an oxygen exchange layer, determining the oxygen deficiency in the HfO_x film, crucial for RRAM operations and switching [5]. A preliminary forming operation is performed by imposing a current compliance I_C=50μA. After forming, which sets the device to LRS, one hundred complete DC switching cycles

Manuscript received January 2014.

F. M. Puglisi and P. Pavan are with Dipartimento di Ingegneria "Enzo Ferrari", Università di Modena e Reggio Emilia, Via P. Vivarelli 10 int. 1, 41125, Modena (MO) - Italy (email: francescomaria.puglisi@unimore.it; phone: +39-059-2056324).

A. Padovani and L. Larcher are with Dipartimento di Scienze e Metodi dell'Ingegneria, Università di Modena e Reggio Emilia, Via Amendola 2, 42122, Reggio Emilia (RE) - Italy.

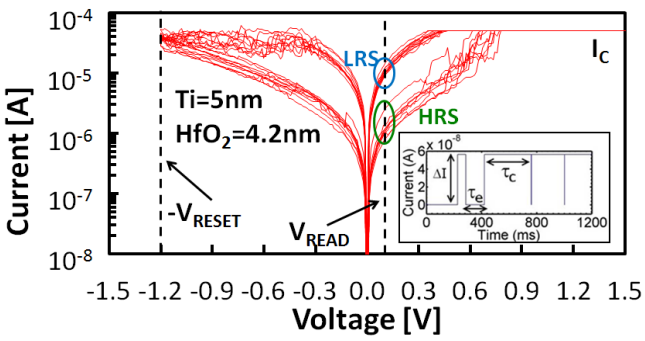

Figure 1. Experimental I-V curves measured at consecutive switching cycles on a TiN/Ti/HfOx/TiN for I_C=50μA and V_{RESET}=1.2V, displaying cycle-to-cycle I_{HRS} and I_{LRS} variability. Also the reset voltage, V_{RESET}, (i.e. the maximum absolute value of the voltage during the reset sweep) and the read voltage, V_{READ}, are highlighted. In the inset, an example of a simple (two-level) RTN, related to a single trap. The different current levels are due to the different states (active/unactive) of a trap within the barrier. Statistical parameters of a single two-level RTN fluctuation are shown (ΔI, τ_C, τ_E).

(set-reset-read) are performed. I-V curves during switching cycles are measured using the Agilent 4155B semiconductor parameter analyzer, Fig. 1, which is used to bias the device when monitoring the RTN current fluctuations, and to collect RTN data as well. Measurements did not show any area dependence, confirming the localized nature of charge transport (not shown). The RTN is measured in RRAM devices cycled using different reset voltages. At every set/reset cycle, the current-time traces are acquired at different read voltages by collecting 10k samples. Noise data are processed through the statistical FHMM method [17, 18], which allows decomposing the multi-level fluctuations into a superposition of two-level signals, each attributed to the activity of an individual defect. This allows characterizing every defect contributing to the multilevel RTN [17, 18]. In this work we focus on the analysis of RTN in HRS, which shows wider normalized fluctuations than LRS [11].

III. Analysis of RTN in the HRS Current

The reset operation is believed to be due to the re-oxidation of the bottom tip of the CF, induced by the oxygen ions diffusion and recombination with the O vacancies [6, 20-23]. This leads to the creation of a dielectric barrier, responsible for the relatively low current observed in HRS. Increasing reset voltage results in the formation of a thicker barrier, which leads to an exponentially higher resistance, R_{HRS} [20-23].

The HRS current, I_{HRS}, is thus due to the electron TAT through the O vacancies (not recombined during the reset operation) in the dielectric barrier [5, 7]. The HRS current is controlled by both barrier thickness, t_B, and the density of the defects within the barrier, which are calculated from the static I-V data using the compact model in [20, 21].

Currently, the physical mechanism responsible for RTN current fluctuations is still unclear. Nevertheless, there are evidences indicating that RTN results from the activation and de-activation of defects assisting the TAT charge transport in the barrier, as we will show later. The defects contributing to RTN are characterized through an FHMM analysis, which we proposed as an effective tool to overcome the limitations of HMM when dealing with multi-level RTN [17, 18]. The FHMM approach allows decomposing the multi-level RTN into independent two-level fluctuations, each corresponding to the activity, i.e., activation and de-activation, of an individual defect. This allows deriving the statistical distribution of the RTN current fluctuations (ΔI), and the capture (τ_c) and emission times (τ_e), see the inset in Fig. 1.

IV. RTN Dependence on the Reset Voltage and Correlation with Cycling Variability

In this Section, we present and discuss the results derived from the statistical analysis of the RTN fluctuations of the HRS current. In particular, we will focus on both the dependence of RTN characteristics on the reset voltage and their correlation with the cycling variability.

A. RTN Dependence on the Reset Voltage

In order to investigate the effect of the reset voltage on the RTN current fluctuations, we evaluated the RTN noise characteristics (ΔI, ΔI/I, τ_c, τ_e) on RRAM devices reset at different voltages, Figs. 2 and 3. As expected, ΔI is log-normally distributed due to the normal variations of the barrier thickness. These are originated by the intrinsic randomness of both diffusion and recombination of the oxygen ions with oxygen vacancy defects during reset. The ΔI distribution rigidly shifts with increasing V_{RESET} since the average I_{HRS} current lowers due to the increase of the barrier thickness. Thus, the amplitude of the average current fluctuation exponentially reduces with increasing reset voltage, Fig. 2c, reflecting the tunnel probability decrease due to the larger barrier thickness. Interestingly, the normalized ΔI/I distribution (I is the average current) is unaffected by the reset voltage, Fig. 2b, thus indicating a strong *statistical* correlation between I and ΔI. This is consistent with the idea that the current I_{HRS} is given by the trap-assisted tunneling through a relatively small number of defects in the barrier. This excludes charge trapping at the interfacial defects between the CF and the surrounding oxide (which is expected to be responsible for RTN current fluctuations in LRS) as the reason for the observed RTN fluctuations in HRS. The current driven by a single defect, ΔI, is thus expected to reduce proportionally to the average current. The ΔI distribution shifts rigidly toward higher current levels with the temperature, Fig. 2d, consistently with the strong temperature dependence of the TAT charge transport. Conversely, the ΔI/I distribution, Fig. 2e, is unaffected by temperature, as both I and ΔI are governed by the same temperature dependence. The effect of the local temperature increase in the dielectric barrier due to the Joule heating is neglected because of the very low electric field applied in reading conditions. So, the internal temperature in the barrier is the same of the environmental one. The resolution of the ΔI/I distributions in Figs. 2b,e is limited by the instrumentation sensitivity, which reduces when measuring small current fluctuations on top of a large average current.

The lognormal behavior of the ΔI distributions is accurately reproduced by the statistical simulations of the HRS current variations performed through the MDLab package [24], Fig.

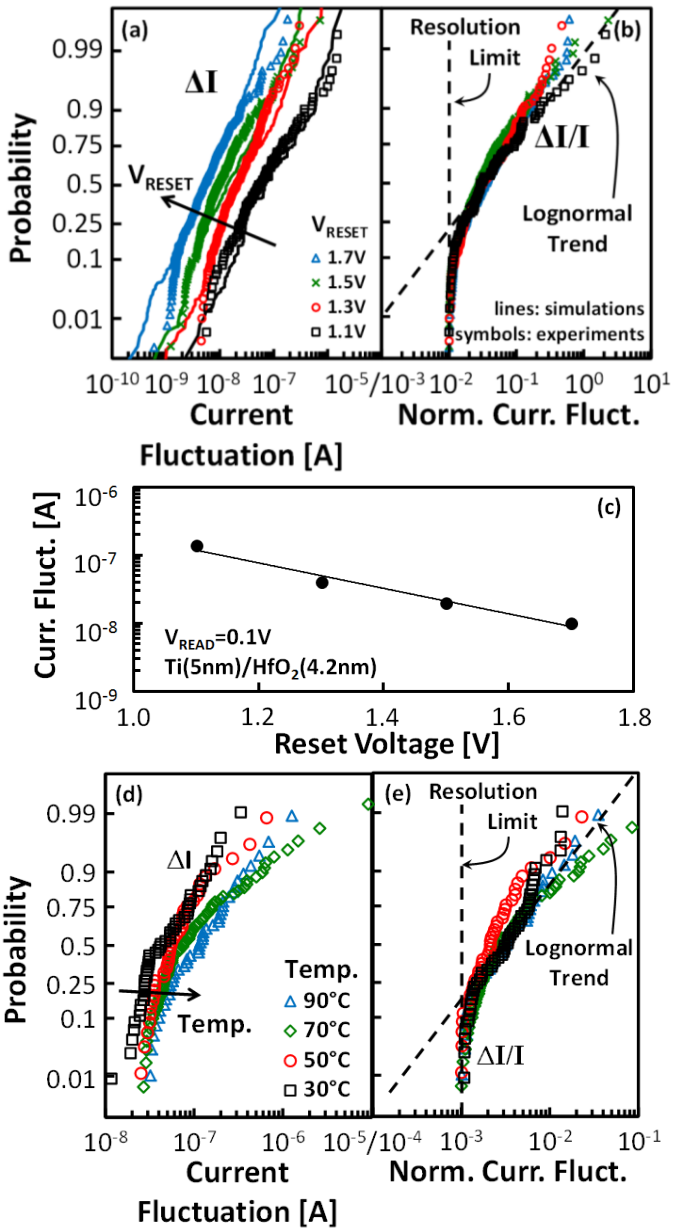

Figure 2. (a) Experimental (upper left plot, symbols) and simulated (lines) ΔI probability distributions for different V_{RESET}. The constant slope of the ΔI distribution indicates that the defect distribution in the barrier is uniform and its density is unaffected by V_{RESET}. (b) Experimental ΔI/I probability distributions (upper right plot, symbols) for different V_{RESET}. The resolution limit of the parameter analyzer, introducing distortions from a pure lognormal trend, is highlighted. (c) The average value of each ΔI distribution is plotted vs. V_{RESET} (circles), along with exponential fitting (solid line). Measurement conditions and sample info are also reported. d) Experimental ΔI and e) ΔI/I probability distributions for a device read at different temperatures.

2a. The HRS current is due to the contributions driven by individual oxygen vacancies, Vo, supporting the electron TAT, which is the dominant charge transport mechanism in the re-oxidized CF tip (dielectric barrier) [5, 7, 11, 13, 20]. We simulated the average HRS current by considering a uniform distribution of Vo defects within the dielectric barrier [5]. The cross-section (≈3-5nm^2 when I_C=50μA and the CF resistivity ρ_{CF}=10kΩ·nm [5]) and the thickness of the barrier are calculated from I-V curves through the compact model in [20, 21]. The defect density considered in these simulations,

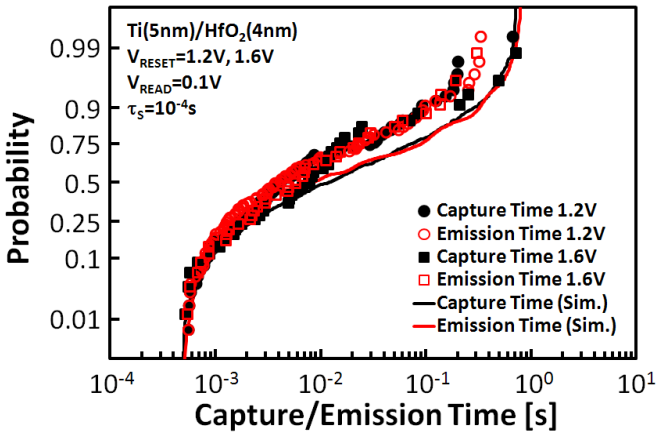

Figure 3. Experimental (symbols) and simulated (lines) capture (black) and emission (red) times probability distributions for different V_{RESET} (different symbol shape), showing good agreement. The details of the experiment are reported in the figure.

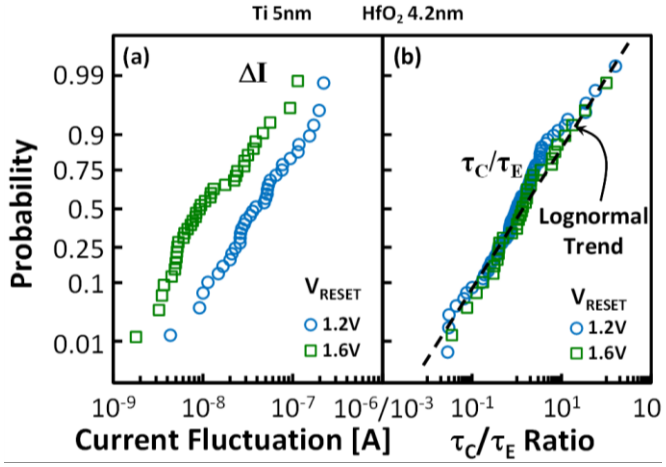

Figure 4. (a) Experimental ΔI (left plot) and (b) τ_C/τ_E ratio (right plot) probability distributions for different V_{RESET}. Lognormal trend (dashed line) is also reported for the τ_C/τ_E ratio. The device is a TiN/Ti/HfO_2/TiN RRAM with a 5nm Ti layer and a 4.2 nm HfO_2 layer, as reported in the figure.

N_T=2·10^{21}cm^{-3}, is consistent with the value independently calculated for RRAM in [25]. The distribution of RTN current fluctuations is simulated by calculating the current variation due to the de-activation of one Vo defect at a time. For full statistics, simulations are repeated for a number of realizations of the random distribution of Vo within the barrier. Figure 3 shows the $\tau_{c,e}$ distributions as extracted with the FHMM algorithm from RTN traces measured on RRAM devices reset at different voltages, i.e. V_{RESET}=1.2V and 1.6V. Regardless the reset voltage, τ_c and τ_e show a log-normal distribution which is correctly reproduced by TAT simulations considering the same defect density used in ΔI simulations - the details of the simulations are described in the Section V. Although the reset voltage affects the distribution of the current fluctuation ΔI, see Fig. 2a, the effect on the RTN capture and emission times is negligible, and the τ_c/τ_e ratio distribution, Fig. 4, exhibits a lognormal behavior independent from the reset conditions.

B. RTN correlation with cycling variability

Since the RTN fluctuations are measured at consecutive set/reset cycles, one could wonder about the correlation

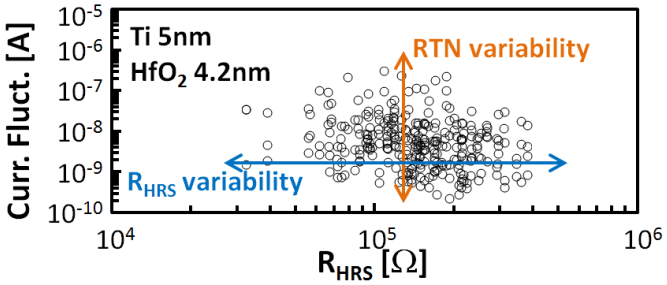

Figure 5. Scatter plot of overall RTN current fluctuation as experimentally retrieved and R_{HRS} over cycling. Similar R_{HRS} can correspond to different current fluctuations, highlighting the uncorrelation between RTN and R_{HRS} variabilities. Reset voltage, V_{RESET}, is 1.5V. Read voltage, V_{READ}, is 0.1V. The Pearson correlation coefficient is -0.136, indicating no direct relation between the amplitude of the current fluctuations and the resistance level.The negative sign is consistent with the statistical trend in Fig. 2a.

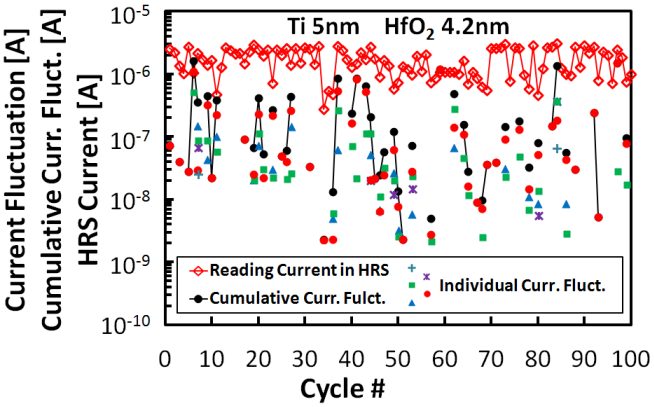

Figure 6. HRS reading current (red line and diamonds), current fluctuation due to each trap contributing to RTN (colored symbols, different colors represents different traps revealed in the same cycle) and cumulative current fluctuation due to the superposition of all traps (black stars and line) extracted from the multi-level RTN I-time traces in HRS through the FHMM technique at each cycle. Reset voltage, V_{RESET}, is 1.1V. Read voltage, V_{READ}, is 0.1V. Missing points in current fluctuation indicate that no RTN (only gaussian noise) was detected at that cycle.

between the RTN results and the cycling variability, whose effect should not be confused with the RTN one. The cycling variability originates from the intrinsic randomness of the reset process, which affects the properties of the CF in the HRS (i.e. the thickness and the defect distribution in the oxidized CF tip), leading to the I_{HRS} variability, Fig. 1. In order to study the statistical correlation between RTN and the I_{HRS} cycling variability, we analyzed the RTN current fluctuations (in reading conditions) and I_{HRS} (or, equivalently, R_{HRS}) at 100 consecutive switching cycles. Figure 5 shows a scatter plot of the HRS resistance and the overall RTN current fluctuations (calculated as the difference between the maximum and the minimum value of the current in the RTN trace) extracted from raw noise data at each cycle with V_{RESET}=1.5V. Different fluctuation amplitudes are found for similar HRS resistance values, indicating that the R_{HRS} variations during cycling are not *directly* correlated to the RTN current fluctuations, Fig. 5. Likewise, the same trend is found by decomposing (using the FHMM technique) the overall multi-level RTN trace in multiple two-level fluctuations, which are associated with the activity of individual traps, Fig. 6. No point-to-point relations are found

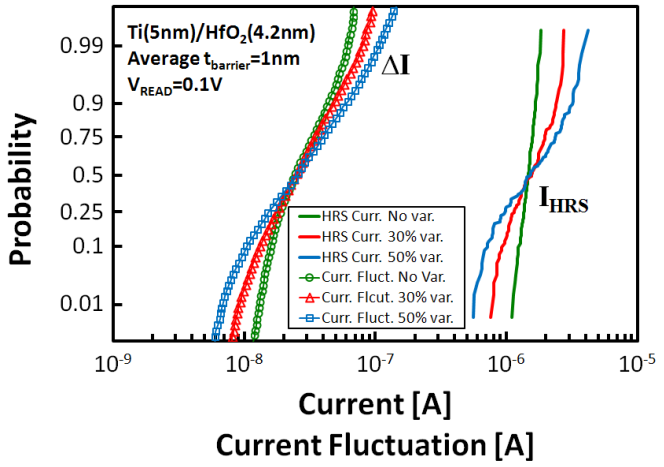

Figure 7. Simulated ΔI (thin lines and symbols, left) and average HRS current I_{HRS} (thick lines, right) distributions over cycling considering a random defects distribution within the dielectric barrier. Green circles/line correspond to a fixed barrier thickness = 1nm. If barrier thickness variations are introduced (red triangles/line = 30% variation and blue squares/line = 50% variation) average HRS current and ΔI show a wider distribution.

between the HRS current and the amplitudes of the individual two-level current fluctuations, ΔI. It is worth noticing that the number of defects detected by the FHMM algorithm at each cycle shows some random variations. Also the cumulative current fluctuation, calculated by summing up the amplitude of every individual two-level fluctuations detected through the FHMM, shows some statistical variations, indicating that there is no point-to-point relation between the current fluctuation amplitudes and the average current. This indicates that two distinct physical mechanisms are responsible for I_{HRS} and RTN fluctuations. Indeed, the HRS current variability is mainly due to the variations of the barrier thickness and the redistribution of the TAT-supporting defects over cycling. Conversely, the RTN current fluctuations are due to the random activation and de-activation of the TAT supporting defects within the barrier. However, barrier thickness variations and the redistribution of the TAT-supporting defects over cycling have a statistical effect on the RTN fluctuations, as confirmed by Monte-Carlo simulations in Fig. 7.

V. Physical Mechanism Responsible for RTN in HRS

In order to clarify the nature of the defects and processes involved in RTN, we analyzed the effect of the read voltage, V_{READ}, on the RTN characteristics extracted through the FHMM algorithm. Here, no switching is performed between consecutive reading operations to prevent any change in both the defect distribution and the thickness of the oxidized CF tip.

Figure 8a shows the average values of ΔI and ΔI/I distributions: ΔI increases with the read voltage, whereas ΔI/I remains constant, confirming that ΔI is due to the activation and de-activation of individual defects supporting the TAT current. The ΔI increase with V_{READ} is due to the higher tunneling and relaxation probabilities. The average RTN capture time raises exponentially, Fig. 8b, whereas the emission time is not affected by V_{READ}. In order to understand these trends we have to speculate about the microscopic mechanisms responsible for the activation and de-activation of

the O vacancy defects supporting TAT [11-13]. This could be due to:

i. a reversible change of the properties of TAT defects due to switching between "slow" atomic configurations, possibly involving metastable states [26];
ii. charge trapping at slow defects located in the proximity of the TAT ones, which could inhibit the electron transport due to the Coulomb blockade effect [27].

Both above mechanisms involve a charge trapping process, which can be described in the framework of the multi-phonon TAT theory. To simplify the analysis, we adopted the compact model presented in [28], where the main parameters are represented by the thermal ionization, E_T, and the relaxation, E_{REL}, energies of the defects, which are typically associated with their specific atomic configuration and with the interaction between electrons and phonons [29].

$$\tau_c = c_0 N_C e^{\left(\frac{x_T}{\lambda_c}\right)} e^{\left(\frac{E_c(V_{READ})}{kT}\right)} \quad (1)$$

$$\tau_e = c_0 N_V e^{\left(\frac{t_B - x_T}{\lambda_c}\right)} e^{\left(\frac{E_e}{kT}\right)} \quad (2)$$

$$E_c = \frac{\left[E_{REL} - \left(E_T - \varphi_B + qV_{READ}\frac{x_T}{t_B}\right)\right]^2}{4E_{REL}} \quad (3)$$

$$E_e = \frac{E_{REL}}{4} \quad (4)$$

Here $\tau_{c,e}$ is the capture (emission) time, c_0 the defect capture cross-section, $N_{c,v}$ the density of states in the source (destination) electrode, x_T the trap distance from the injecting electrode, E_T the trap ionization energy, E_{REL} the relaxation energy, t_B the barrier thickness, $\lambda_{c,e}$ the tunneling constant for the capture (emission) process, k the Boltzmann constant, T the absolute temperature, φ_B the energy offset at the electrode/oxide interface, V_{READ} the read voltage. In the framework of this simple compact model, the capture and emission times are calculated by neglecting the back-emission to the injecting electrode. This does not affect the result accuracy, as the Vo defects mostly contributing to the TAT current lie in the middle of the barrier [7] (including the back-emission results in no significant difference in the calculated $\tau_{c,e}$). Indeed, this compact description allows correctly reproducing the experimental trends of capture and emission times vs. read voltage shown in Fig. 8b. The τ_c raise with increasing V_{READ} is mainly due to the higher energy released by electrons to the lattice at every capture event. Regarding this point, it is important to highlight that τ_c may either increase or decrease with the read voltage, depending on the energy misalignment between the electrons and the defect. If the ground state of the defect has a thermal ionization energy higher (lower) than the Fermi level, $E_T < \varphi_B$ ($E_T > \varphi_B$), τ_c increases (reduces) with the voltage , according to eqn. (1,3). Conversely, the constant trend shown by τ_e is due to the fact that the electron emission occurs preferentially from the

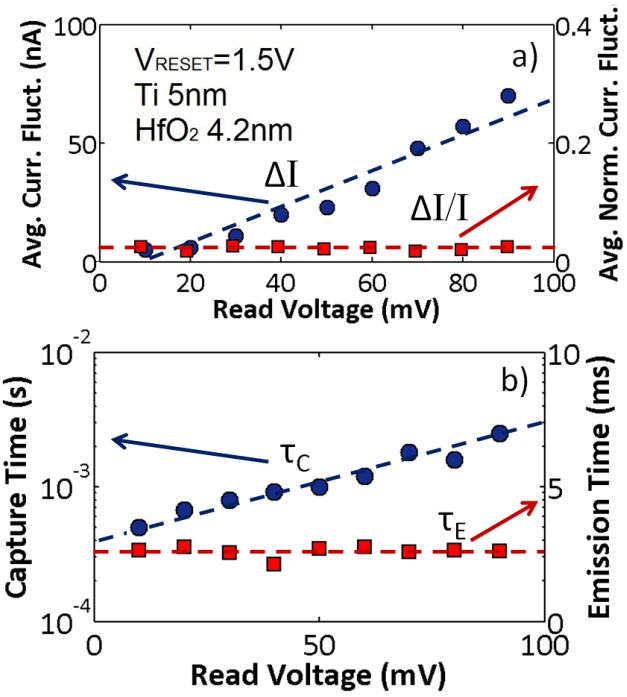

Figure 8.(a) Experimental ΔI (left y-axis, blue circles) and ΔI/I (right y-axis, red squares) average values for different V_{READ}. ΔI scales with the average current I. (b) Experimental capture (left y-axis, blue circles) and emission (right y-axis, red squares) times average values for different V_{READ}. Capture time exponentially depends on the read voltage while emission time shows no dependency, in agreement with the TAT model.

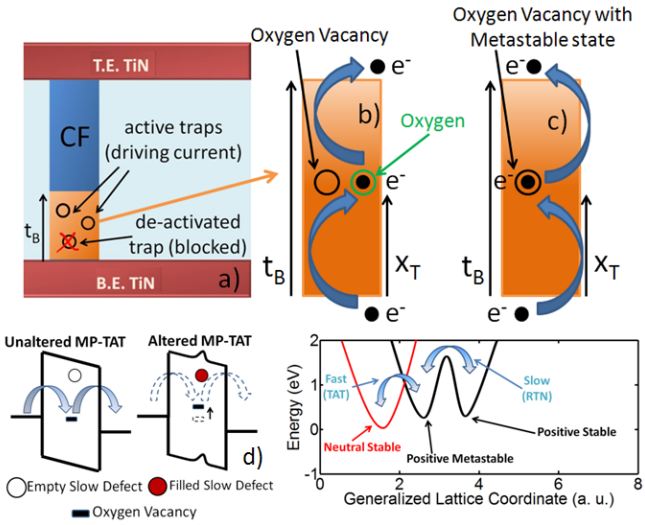

Figure 9. (a) Schematic of the device in HRS. (b,c) The representation of two mechanisms possibly responsible for the RTN. The barrier thickness and the trap location are highlighted. (b) Charge trapping at a slow defect (in green, probably the O interstitial) may induce a Coulomb blockade effect on a close O vacancy, normally assisting the TAT transport. (c) O vacancy activation and de-activation through metastable state configurations of the O vacancy. (d) Schematic illustration of the Coulomb blockade. The charge trapping at the slow defect in the proximity of the O vacancy changes the potential and the energy alignment of the O vacancy, altering the associated TAT current. (e) Generalized coordination diagram illustrating the O vacancy model with metastable states. The TAT current involves the charge transition between the neutral and the positive metastable state. The RTN is generated by the relaxation of the positive metastable state into a stable configuration. This process temporarily inhibits the TAT transport and causes RTN.

ground state of the trap, hence the relaxation probability is not affected by changes in the applied voltage [7]. To reproduce both average trends, Fig. 8b, and the statistical distributions of

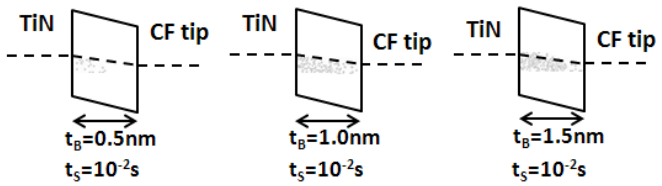

Figure 10. Schematic representation of the band diagram of the analyzed region of the device. Defect states in the bandgap of the HfO_x barrier may result in detectable RTN fluctuations. Calculations are reported for different barrier thicknesses (0.5nm, 1.0nm, and 1.5nm) and include defects generating RTN signals which can be measured with a sampling time t_s=10ms. The dashed line represents the Fermi level. More defects may be involved in RTN as the barrier thickness increases.

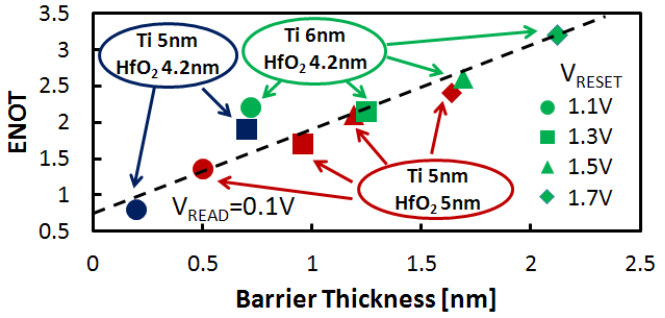

Figure 11. ENOT (symbols) vs. average barrier thickness for different device stacks reset at different V_{RESET} along with linear fitting (line). Increasing barrier thickness results in increasing statistical complexity of RTN.

capture and emission times, Fig. 6, the relaxation energy has been considered as a fitting parameter, as the value calculated (E_{REL}=1.2eV) for positively charged O vacancy defects [29-31] leads to very fast capture and emission events (responsible for the TAT current) in the nanoseconds to picoseconds range. Instead, the capture and emission times observed in RTN fluctuations are orders of magnitude larger, Fig. 3. This rules out the hypothesis that charge trapping at positively charged oxygen vacancies may be responsible for RTN [30]. The relaxation energy extracted from the capture and emission times simulations in Fig. 3, E_{REL}=1.8-2.7eV, is indeed larger than that of O vacancies assisting the TAT [7], probably indicating that a different atomic species or arrangement is responsible for RTN [29]. In this respect, a possible candidate is given by the neutral interstitial oxygen, an electrically active defect in HfO_2 showing similar thermal ionization and relaxation energy values to the one extracted from RTN simulations [31]. This would support the hypothesis ii) that the charge trapping at neutral oxygen interstitial prevents an O vacancy in its close proximity to effectively support the TAT transport due to the Coulomb blockade effect, as sketched in Fig. 9b,d. Despite simulations considering trapping at nearby interstitial oxygen [31] ($N_{T,IntOx}$=$5\cdot10^{20}$cm^{-3}) were shown to accurately reproduce the experimental RTN current fluctuations [32], further studies are needed to assess the microscopic characteristics of such defects, i.e., their thermal ionization and relaxation energies.

On the other hand, also the existence of metastable states has still to be assessed for O vacancy defects in HfO_2 [26]. Metastable states correspond to different electron cloud arrangements around the atoms surrounding the defect. Their properties were calculated for *E'* centers in SiO_2 using ab-initio calculations [26]. Similar techniques could be applied to HfO_2, but further studies are required to reach unambiguous conclusions. Nevertheless, this assumption represents another possible physical mechanism for RTN in RRAM devices. In this framework, the transition of the O vacancy defect from a metastable (i.e. fast) to a stable (i.e. slow) state configuration can de-activate the charge transport through the defect (and vice versa), thus explaining the RTN current fluctuations. When the defect is in its metastable configuration, the captured electron will be promptly emitted: the time constant of the process is thus very small, and the electron trapping and emission contribute to the leakage current. Conversely, when the defect is in its stable configuration, the capture and emission times are much longer, and therefore the defect is not able to further assist charge transport, Fig. 9c,e.

VI. Considerations

The interpretation of the RTN data extracted through the FHMM analysis allows gaining useful insights into both the physical processes and the defect species involved in RTN.

It is important to underline that defects contributing to detectable RTN current fluctuations have to be aligned with the Fermi level. Capture and emission times should indeed be comparable to allow the detection of both raising and falling edges of the current fluctuations (i.e. very dissimilar values of capture and emission times will impede the detection). Furthermore, such defects are required to be located in a given portion of the barrier, which also depends on the barrier thickness. This is shown in the band diagram plot depicted in Fig. 10, which maps the portion of the dielectric band-gap that can be inspected using noise measurements. Interestingly, a thicker barrier results in a relatively larger portion of the barrier hosting defects which may contribute to RTN. The total number of defects is thus expected to increase with V_{RESET}, as well as the "statistical complexity" of the RTN signal, when statistically observed over multiple switching cycles. The statistical complexity is evaluated through a figure of merit named "effective number of traps" (ENOT). ENOT is calculated by averaging the effective number of defects contributing to RTN detected at consecutive set-reset cycles through the FHMM algorithm [33-35]. The barrier thickness at each cycle is extracted from I-V data using the compact model in [20, 21]. Despite no point-to-point correlation exists between HRS resistance (i.e. barrier thickness) variations and RTN current fluctuations, Fig. 6, a linear correlation is found between the ENOT and the barrier thickness, as more defects are expected to contribute to RTN, Fig. 11. The same trend is observed in devices with different stacks reset at different voltages. The linear relation between the average barrier thickness and the ENOT follows a sort of universal law, which indicates that the defect density in the barrier does not depend on the stack composition and the reset voltage [25, 36]. Most probably it is a property of the material at a given sub-stoichiometry level. This result, consistent with the results of the simulations in Fig. 10, indicates that understanding the physical properties of the material is crucial for controlling noise behavior and variability in RRAM devices [37-41].

Possibly, materials with low fractional oxygen content and/or high lattice "flexibility" (the capability to rearrange the lattice upon some defects creation) may constitute a preferential choice to limit the concentration of defects involved in RTN. Nevertheless, a detailed analysis must be performed on any material to fully identify the defects responsible for RTN.

VII. Conclusion

In this paper we presented the results of a complete statistical characterization of multi-level RTN in HfO_2 RRAM devices in HRS. The statistical properties of the RTN current fluctuations have been analyzed through the FHMM technique. This allows decomposing the multi-level RTN fluctuations into many two-level signals, each associated with an individual defect in the oxidized tip of the CF. A consistent picture of the RTN fluctuations in HRS in the framework of the TAT theory has been proposed. RTN is attributed to the activation and de-activation of TAT-supporting O vacancy defects. These processes can be due to either the presence of metastable state configurations for the O vacancy defects or the Coulomb interaction with the charge trapped at defects of different nature. Results point to the interstitial oxygen as a possible candidate. The uncorrelated nature of cycling variability and RTN has been identified and explained. Moreover, a systematical analysis of I-V data considering cycling variability and RTN in devices with different stack configurations allowed confirming the statistical link between noise behavior and the dielectric barrier properties.

Acknowledgment

The authors wish to thank Sematech for providing samples.

References

[1] Y.-B. Kim et al., "Bi-layered RRAM with unlimited endurance and extremely uniform switching", Symposium on VLSI Technology (VLSIT) 2011, pp.52,53, 14-16 June 2011.

[2] X. P. Wang et al., "Highly compact 1T-1R architecture ($4F^2$ footprint) involving fully CMOS compatible vertical GAA nano-pillar transistors and oxide-based RRAM cells exhibiting excellent NVM properties and ultra-low power operation", IEEE International Electron Devices Meeting (IEDM) 2012, pp.20.6.1,20.6.4, 10-13 Dec. 2012.

[3] J. Lee et al., "Diode-less nano-scale ZrOx/HfOx RRAM device with excellent switching uniformity and reliability for high-density cross-point memory applications", IEEE International Electron Devices Meeting (IEDM) 2012, pp.19.5.1,19.5.4, 6-8 Dec. 2010.

[4] X. A. Tran et al., "High performance unipolar AlOy/HfOx/Ni based RRAM compatible with Si diodes for 3D application", Symposium on VLSI Technology (VLSIT) 2011, pp.44,45, 14-16 June 2011.

[5] G. Bersuker et al., "Metal oxide resistive memory switching mechanism based on conductive filament properties", Journal of Applied Physics vol.110, no.12, pp.124518,124518-12, Dec. 2011.

[6] A. Kalantarian et al., "Microscopic model for the kinetics of the reset process in HfO2 RRAM", International Symposium on VLSI Technology, Systems, and Applications (VLSI-TSA) 2013, pp.1,2, 22-24 Apr. 2013.

[7] L. Vandelli et al., "A Physical Model of the Temperature Dependence of the Current Through SiO_2/HfO_2 Stacks", IEEE Transactions on Electron Devices, vol.58, no.9, pp.2878,2887, Sept. 2011.

[8] S. Long et al., "Compact analytical models for the SET and RESET switching statistics of RRAM inspired in the cell-based percolation model of gate dielectric breakdown", IEEE International Reliability Physics Symposium (IRPS) 2013, pp.5A.6.1,5A.6.8, 14-18 April 2013.

[9] A. Chen and M.-R. Lin, "Variability of resistive switching memories and its impact on crossbar array performance", IEEE International Reliability Physics Symposium (IRPS) 2011, pp.MY.7.1,MY.7.4, 10-14 April 2011.

[10] X. Guan et al., "A SPICE Compact Model of Metal Oxide Resistive Switching Memory With Variations", IEEE Electron Device Letters, vol.33, no.10, pp.1405,1407, Oct. 2012.

[11] D. Veksler et al., "Methodology for the statistical evaluation of the effect of random telegraph noise (RTN) on RRAM characteristics", IEEE International Electron Devices Meeting (IEDM) 2012, pp.9.6.1,9.6.4, 10-13 Dec. 2012.

[12] F. M. Puglisi et al., "Random Telegraph Signal noise properties of HfOx RRAM in high resistive state", Proceedings of the European Solid-State Device Research Conference (ESSDERC) 2012, pp.274,277, 17-21 Sept. 2012.

[13] F. M. Puglisi et al., "RTS noise characterization of HfOx RRAM in high resistive state", Solid-State Electronics, vol. 84, pp. 160-166, Jun. 2013, ISSN 0038-1101.

[14] D. Ielmini, F. Nardi, C. Cagli, "Resistance-dependent amplitude of random telegraph-signal noise in resistive switching memories", Applied Physics Letters , vol.96, no.5, pp.053503,053503-3, Feb 2010.

[15] N. Raghavan et al., "Microscopic origin of random telegraph noise fluctuations in aggressively scaled RRAM and its impact on read disturb variability", IEEE International Reliability Physics Symposium (IRPS) 2013, pp.5E.3.1,5E.3.7, 14-18 Apr. 2013.

[16] Z. Fang et al., "Low-Frequency Noise in Oxide-Based TiN/HfOx/Pt Resistive Random Access Memory Cells", IEEE Transactions on Electron Devices, vol.59, no.3, pp.850,853, Mar. 2012

[17] F. M. Puglisi, P. Pavan, "RTN analysis with FHMM as a tool for multi-trap characterization in HfOX RRAM", Proceedings of IEEE International Conference on Electron Devices and Solid-State Circuits (EDSSC) 2013, pp.1,2, 3-5 June 2013.

[18] F. M. Puglisi, P. Pavan, "Factorial Hidden Markov Model analysis of Random Telegraph Noise in Resistive Random Access Memories", ECTI Transactions on Electrical Engineering, Electronics, and Communications, vol. 12, no.1, pp. 24-29, 2014.

[19] J. Martin-Martinez et al., "New Weighted Time Lag Method for the Analysis of Random Telegraph Signals", IEEE Electron Device Letters, vol.35, no.4, pp.479,481, April 2014.

[20] F. M. Puglisi et al., "An Empirical Model for RRAM Resistance in Low- and High-Resistance States," IEEE Electron Device Letters, vol.34, no.3, pp.387,389, March 2013.

[21] F. M. Puglisi, P. Pavan, A. Padovani, L. Larcher, "A compact model of hafnium-oxide-based resistive random access memory", Proceedings of IEEE International Conference on IC Design & Technology (ICICDT) 2013, pp.85,88, 29-31 May 2013.

[22] S. Yu, H. –S. P. Wong, "A Phenomenological Model for the Reset Mechanism of Metal Oxide RRAM", IEEE Electron Device Letters, vol.31, no.12, pp.1455,1457, Dec. 2010.

[23] T. Diokh et al., "Investigation of the impact of the oxide thickness and RESET conditions on disturb in HfO2-RRAM integrated in a 65nm CMOS technology", IEEE International Reliability Physics Symposium (IRPS) 2013, pp.5E.4.1,5E.4.4, 14-18 Apr. 2013.

[24] http://www.mdlab-software.com

[25] J. Robertson, R. Gillen, "Defect densities inside the conductive filament of RRAMs", Microelectronic Engineering, vol. 109, pp. 208-210, Sept. 2013, ISSN 0167-9317.

[26] T. Grasser, "Stochastic charge trapping in oxides: From random telegraph noise to bias temperature instabilities", Microelectronics Reliability vol. 52(1), pp. 39-70, 2012.

[27] F. M. Puglisi et al., "Instability of HfO2 RRAM devices: comparing RTN and cycling variability", Proceedings of the IEEE International Reliability Physics Symposium (IRPS) 2014, MY. 5.1-MY. 5.5, 1-5 June 2014.

[28] L. Larcher, A. Padovani, P. Pavan, "Leakage current in HfO2 stacks: from physical to compact modeling", NSTI-Nanotech 2012, vol. 2, pp. 809.

[29] N. Capron, P. Broqvist, A. Pasquarello, "Migration of oxygen vacancy in HfO2 and across the HfO2/SiO2 interface: A first-principles investigation", Applied Physics Letters, 91, 192905 (2007).

[30] D. Muñoz Ramo et al., "Spectroscopic properties of oxygen vacancies in monoclinic HfO_2 calculated with periodic and embedded cluster density functional theory", *Phys. Rev. B, Condens. Matter*, vol. 75, no. 20, p. 205 336, May 2007.

[31] A. S. Foster et al., "Vacancy and interstitial defects in hafnia", *Phys. Rev. B, Condens. Matter*, vol. 65, no. 17, p. 1744 117, May 2002.

[32] F. M. Puglisi et al., "A microscopic physical description of RTN current fluctuations in HfOx RRAM", to be presented at IEEE IRPS 2015, 21-23 Apr. 2015.

[33] F. M. Puglisi et al., "Random Telegraph Noise analysis to investigate the properties of active traps of HfO2-Based RRAM in HRS", Proceedings of the European Solid-State Device Research Conference (ESSDERC) 2013, pp.166-169, 16-20 Sept. 2013.

[34] F. M. Puglisi, P. Pavan, "An investigation on the role of current compliance in HfO2-based RRAM in HRS using RTN and I-V data", 15th International Conference on Ultimate Integration on Silicon (ULIS) 2014, pp.129,132, 7-9 Apr. 2014.

[35] F. M. Puglisi, P. Pavan, A. Padovani, L. Larcher, "A study on HfO2 RRAM in HRS based on I-V and RTN analysis", Solid-State Electronics, vol. 102, pp. 69-75. Dec. 2014.

[36] L. Larcher et al., "A Compact Model of Program Window in HfOx RRAM Devices for Conductive Filament Characteristics Analysis", IEEE Transactions on Electron Devices, vol.61, no.8, pp.2668-2673, Aug. 2014.

[37] N. Raghavan et al., "RTN insight to filamentary instability and disturb immunity in ultra-low power switching HfOx and AlOx RRAM", Symposium on VLSI Technology (VLSIT) 2013, pp.T164,T165, 11-13 June 2013.

[38] Y. Zhang et al., "Random telegraph noise analysis in AlOx/WOy resistive switching memories", Applied Physics Letters, vol.104, no.10, pp.103507,103507-4, Mar 2014.

[39] J. K. Lee et al., "Extraction of trap location and energy from random telegraph noise in amorphous TiOx resistance random access memories", Applied Physics Letters, vol.98, no.14, pp.143502,143502-3, Apr. 2011.

[40] J. K. Lee et al., "Conduction and Low-Frequency Noise Analysis in Al/α-TiOx/Al Bipolar Switching Resistance Random Access Memory Devices", IEEE Electron Device Letters, vol.31, no.6, pp.603,605, June 2010.

[41] M. Terai et al., "Memory-State Dependence of Random Telegraph Noise of Ta_2O_5/TiO_2 Stack ReRAM", IEEE Electron Device Letters, vol.31, no.11, pp.1302,1304, Nov. 2010.

Francesco Maria Puglisi (S'12) was born in Cosenza, Italy, in 1987. He received the M.Sc. degree in Electronic Engineering in 2010 from University of Calabria, Italy, and the Ph.D. degree in Information and Communication Technology in 2015 from University of Modena and Reggio Emilia, Italy, where he is currently a Research Associate.

His activity focuses on the characterization and compact modeling of novel nonvolatile memories, especially RRAM, focusing on noise and variability.

Dr. Puglisi authored and coauthored more than 20 technical papers. He is the recipient of the Best Student Paper Award at the IEEE ICICDT 2013 Conference, 29-31 May 2013, Pavia, Italy and of the "E. Loizzo" Memorial Award as the best engineering graduate at University of Calabria in the 2010-2012 time span.

Luca Larcher (M'01) received his Ph.D. in Information Engineering in 2001 from the University of Modena and Reggio Emilia, where he is currently Associate Professor.

His research interests concern the characterization and physical modeling of non-volatile memory devices and charge transport in high-k dielectrics, and the design of CMOS integrated circuits for both communication and energy harvesting.

Prof. Larcher authored a book and more than 150 technical papers. He has joined the technical committees of IEDM (2006-2007, 2013-2015), IRPS (2011-2012) and IIRW (2012-2014) conferences.

Andrea Padovani (S'06–M'10) received the Ph.D. degree in 2010 from the University of Ferrara. He is a co-founder of the MDLab s.r.l. company developing and marketing software solutions for the simulation of micro/nano-electronic devices. He is also an Adjunct Professor at the University of Modena and Reggio Emilia, Italy.

His research interests include the modeling of dielectric degradation and breakdown of high-k/metal gate transistors and the modeling of innovative nonvolatile memories (charge-trapping devices and resistive random access memory).

Dr. Padovani authored and coauthored more than 100 technical papers. He currently serves as Committee Member of IEEE IRPS, IEEE IIRW, VLSI-TSA and ESREF conferences.

Paolo Pavan (SM'12) is Professor of Electronics at the University of Modena and Reggio Emilia, Italy, since 1994.

His research interests are in the characterization, modeling and optimization of nonvolatile memory devices and, more recently, in the development of safety critical and energy-aware applications for automotive electronics.

Prof. Pavan was in the IEDM Technical and Executive Committee from 2002 to 2006. He has been Guest Editor of the IEEE Transactions on Device and Material Reliability Special Issue on Nonvolatile Memories in Sept. 2004. He has been in the Technical Committee of VLSI-TSA from 2006 to 2010. He is in the Technical Committee of IRPS 2014; in ESSDERC and ESREF from 2012. He has been Technical Program Chair of ESSDERC 2014 and now in the Steering Board of ESSDERC.